

## Twice reflected ultrasonic bulk wave for surface defect monitoring

Voon-Kean Wong<sup>a,1</sup>, Xiaotian Li<sup>a,1</sup>, Yasmin Mohamed Yousry<sup>a</sup>, Marilyne Philibert<sup>a</sup>, Chao Jiang<sup>a</sup>, David Boon Kiang Lim<sup>a</sup>, Percis Teena Christopher Subhodayam<sup>a</sup>, Zheng Fan<sup>b</sup>, Kui Yao<sup>a,\*</sup>

<sup>a</sup> Institute of Materials Research and Engineering (IMRE), Agency for Science, Technology and Research (A\*STAR), 2 Fusionopolis Way, Innovis #08-03, Singapore 138634, Singapore

<sup>b</sup> School of Mechanical and Aerospace Engineering, Nanyang Technological University, 50 Nanyang Avenue, Singapore 639798, Singapore

### ARTICLE INFO

#### Keywords:

Structural health monitoring  
Surface defect  
Longitudinal wave  
Time-of-flight diffraction (TOFD)  
Piezoelectric  
Ultrasonic transducer

### ABSTRACT

This work offers an ultrasonic structural health monitoring (SHM) approach for assessing the defects located on the same surface and at one side of piezoelectric ultrasonic transducer array. It is based on the analysis of ultrasonic bulk wave travelling in the thickness direction obtained from an enhanced full-skip configuration of the time-of-flight diffraction (TOFD) technique. In contrast to existing TOFD setup only considering the direct paths between the ultrasonic transducer and defect, our ultrasound monitoring configuration involves twice reflected ultrasonic bulk wave (TRBW). The TRBW travels following the propagation route from an ultrasonic transmitter located at the same side of the defect initiated, the backwall, the defect tip, the backwall again and finally to the same or another ultrasonic transducer. Both theoretical analyses and experimental validations have been conducted in our study. A simplified algorithm for efficient detection and mapping the growth of a surface defect in an aluminum alloy block has been demonstrated with an incremental surface defect growth starting from 2.80 mm in depth, in which conformable direct-write ultrasonic transducers (DWT) made of in-situ piezoelectric coating are implemented. Our approach provides an ultrasonic method for effective monitoring the near surface defects with the ultrasonic transducers conveniently implemented on the same surface and at the same side of the defects.

### 1. Introduction

Surface defects such as cracks and corrosion are pervasive problems in engineering structures. Timely detection of such defects is important, spurring demand for detecting the initiation and monitoring the growth of these defects. Monitoring critical hotspots proactively can enhance safety by preventing catastrophic failures and extends the lifespan of critical engineering structures. The industry has implemented various structural health monitoring (SHM) methods for this purpose. Ultrasonic SHM is widely employed for monitoring surface defects due to its high sensitivity, accuracy, rapid response, and versatility in both long-distance surface propagation and deep penetration, depending on the implemented ultrasonic wave modality [1,2]. Guided waves are often employed for ultrasonic SHM of thin structures, making use of fundamental modes at lower frequencies where there are fewer overlapping modes. Using lower frequencies or larger wavelengths results in a lower

sensitivity to small defects and typically cannot provide a quantitative result. On the other hand, the Rayleigh wave (a type of surface wave) stands out as the best pick for detecting and monitoring surface defects, due to its concentrated energy near the surface of the structure. However, its applicability is limited by defect depths that correspond to the Rayleigh wavelength [3,4]. In contrast, ultrasonic bulk waves offer a compelling option for monitoring deeper surface cracks, given their propagation direction, which is in the structure's thickness direction [5,6].

The arrival time of a scattered ultrasonic bulk wave from a defect can facilitate defect sizing and localization. A renowned application of ultrasonic bulk wave for defect sizing is the Time-of-Flight Diffraction (TOFD) method, developed by Silk et al. [7] in the late 1970 s. The basic principle of TOFD is shown in Fig. 1. The conventional TOFD method allows sizing of defects by analysing the arrival time of the ultrasonic bulk waves that are diffracted by the tips of the defect presented in the

\* Corresponding author.

E-mail address: [k-yao@imre.a-star.edu.sg](mailto:k-yao@imre.a-star.edu.sg) (K. Yao).

<sup>1</sup> These authors contributed equally to the work.

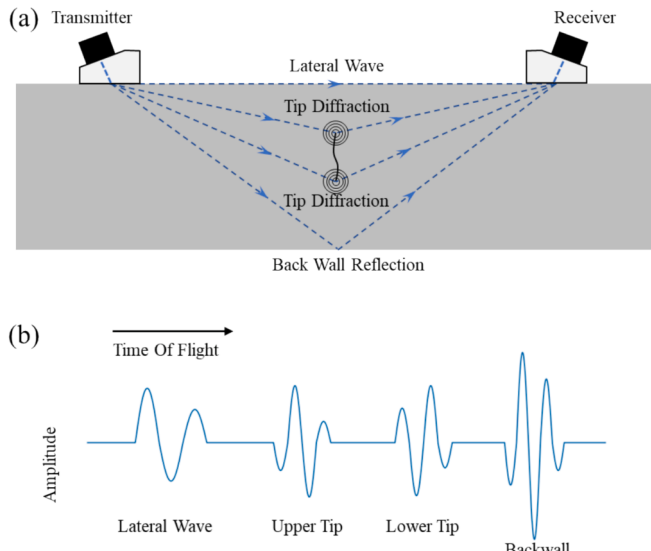


**Fig. 1.** (a) Conventional TOFD setup with indicated wave paths used for depth calculations and crack tips marked as point scatterers; (b) time delay for each signal.

structure, as illustrated in Fig. 1(a). To realize this method, two ultrasonic wave probes with angle wedges are usually used in the pitch-catch mode: one as transmitter, and the other as receiver. This results in the four ultrasonic signals as shown in Fig. 1(b). The first is called the lateral wave, which is the ultrasonic wave propagating in the near surface. Two ultrasonic signals are generated as the ultrasonic bulk wave interacts with the defect presence in the structure, as “upper tip” and “lower tip” diffraction signals. The arrival time difference between the upper tip and lower tip diffraction signals is used to calculate the height of the defect. The fourth signal pertains to the ultrasonic bulk wave reflected from the backwall of the structure.

Yeh et al. [8] presents a method for surface crack depth sizing with TOFD method. This involves ultrasonic transducers with wedge to generate and detect ultrasonic shear bulk waves, with the surface crack between the ultrasonic transducers. Using similar ultrasonic transducer arrangement, Jin et al. [9] summarizes a method for estimating the size of cracks in pipes using TOFD method. These methods require the use of bulky ultrasonic transducers and instrumentation. On the other hand, Ochichai et al. [10] introduces a crack depth sizing technique based on TOFD analysis, with the ultrasonic bulk waves generated and detected using a laser-ultrasonic system. This technique generates and detect ultrasonic bulk wave with a laser-ultrasonic system, thereby requires a clear line-of-sight. [11] Furthermore, the crack is located at the backwall of the structure, deviating from the previous two works of having it on the same surface as the ultrasonic bulk wave transmitter and receiver.

The conventional TOFD methods implement separate ultrasonic bulk wave transmitter and receiver outside of the surface defect, as illustrated in Fig. 1(a). In many actual cases, only one side of the structure is accessible, such as welded T-joints. Thus, monitoring the initiation and growth of a surface defect on the same surface and the same side of the defect is demanded for many applications, but is challenging. Another major limitation of conventional TOFD methods is the presence of near surface dead zone that limits the detection of near surface defects. [1] The near surface dead zone happens because the detection of the lateral wave signal overshadows the tip-diffracted signals from defect, hindering the ability for this method to detect defects near the surface, typically within a depth of 4 mm to 8 mm. Researchers and engineers have attempted to detect defects in the dead zone. Jin et al. [12] developed a corrected mode-converted wave method for detecting defects in TOFD dead zone, but this method still uses two separate transducers placed on different sides of the crack.

Implementing TOFD methods for SHM is hindered primarily by the bulky ultrasonic transducers and coupling issues. In recent developments, the direct-write ultrasonic transducer (DWT) made from piezoelectric coatings has grown in popularity for ultrasonic SHM. [13–15] DWT provides many advantages, including high conformity, lightweight, low-profile, and extra benefits attributed to scalable batch processing. The application of DWT negates the need for bulky ultrasonic transducers, providing a solution for performing in-situ SHM of hotspots within confined spaces. The conformability of DWT onto the structure ensures good acoustic coupling between the DWT and the structure, yielding consistent and reliable ultrasonic signals for SHM applications [16,17]. Leveraging these advantages, this study applies piezoelectric DWT to form an ultrasonic transducer array for effective surface defect localization and depth measurement.

In this study, an improved TOFD method is developed by analysing the TRBW with ultrasonic transducer array made of piezoelectric DWTs on the same side of the crack. The novelty of this work includes:

- Capability of detecting surface defects with the ultrasonic transducers on the same surface and at the same side.
- Solves the issue of detecting near surface defects by ensuring the TRBW's signal is not overshadowed by the lateral wave's signal.
- Implements a simplified algorithm to simultaneously locate the surface defect and measure its depth.
- Enables real-time and reliable defect monitoring by using in-situ fabricated piezoelectric DWTs.

## 2. Surface defect detection and sizing by twice reflected ultrasonic bulk wave

This section discusses the algorithm for detecting surface defects with the ultrasonic transducers located at the same side of the surface defect, as illustrated in Fig. 2. An ultrasonic transducer generates a longitudinal bulk wave, propagating in the thickness direction of the structure underneath. This longitudinal bulk wave is then reflected off the backwall for the first time and propagates towards the surface defect. Upon reaching the tip of the surface defect, the longitudinal bulk wave is diffracted, redirecting part of the ultrasonic wave toward the backwall again. Thereafter, it is reflected off the backwall for the second time, returning to the ultrasonic transducer, where it is subsequently detected. The detected ultrasonic wave is labelled as the twice reflected ultrasonic bulk wave (TRBW).

This method differs from traditional TOFD methods as the ultrasonic bulk wave is reflected by the backwall twice before being received by an ultrasonic transducer. The TRBW method is used here to avoid the two disadvantages of the conventional TOFD. First, since the arrival time of

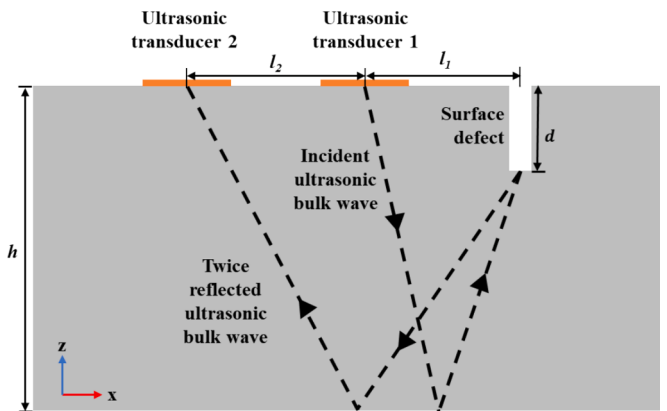


**Fig. 2.** Schematic illustration of the method for using the twice reflected ultrasonic bulk wave (TRBW) to monitor the depth and location of the surface crack on a structure.

the TRBW is greatly extended, the lateral wave's signal would not be shadowing TRBW's signal, thereby solving the near surface dead-zone issue. Second, the ultrasonic transducers are placed at the same side of the crack, simulating actual situations where there is no access to the other side of structure, for instance in welded T-joints.

Two ultrasonic transducers can be placed at the same side of the surface defect without precisely knowing the distance between the surface defect and the ultrasonic transducers, as illustrated in Fig. 2. An algorithm is devised to calculate the surface defect's depth as well as the location of the surface defect. Denoting the arrival time of the TRBW received by ultrasonic transducer 1 (UT1) and ultrasonic transducer 2 (UT2) as  $T_1$  and  $T_2$ , respectively:

$$T_1 = \frac{2\sqrt{l_1^2 + (2h - d)^2}}{c}, \quad (1)$$

$$T_2 = \frac{\sqrt{l_1^2 + (2h - d)^2} + \sqrt{(l_1 + l_2)^2 + (2h - d)^2}}{c}, \quad (2)$$

where,  $l_1$  is the distance between UT1 and the surface defect;  $l_2$  is the distance between UT1 and UT2;  $h$  is the thickness of the structure;  $d$  is the depth of the surface defect; and  $c$  is the velocity of the ultrasonic bulk wave. The distance between UT1 and the crack ( $l_1$ ) and the surface defect depth ( $d$ ) can be solved as:

$$l_1 = \frac{c^2 T_2 (T_2 - T_1)}{2l_2} - \frac{l_2}{2}, \quad (3)$$

$$d = 2h - \frac{1}{2} \sqrt{(cT_1)^2 - \left( \frac{c^2 T_2 (T_2 - T_1)}{l_2} - l_2 \right)^2}. \quad (4)$$

This algorithm assumes that the two ultrasonic transducers are placed at the same side of the crack and only applicable for the 2D situation shown in Fig. 2. If the surface defect is not positioned directly in front of the two ultrasonic transducers in a straight line, additional ultrasonic transducers are required to achieve the 2D configuration shown in Fig. 2 in order to determine the defect's location and subsequently

measure its depth.

### 3. Experimental setup

Experimental studies were carried out to validate the applicability of the proposed TRBW method for determining the location and depth of the surface defect. An aluminum alloy block with dimensions of 150 mm × 150 mm × 38 mm was selected for experimental validation. A schematic showing the top view of the aluminum alloy block, indicating the placement of the ultrasonic transducer array, and of a simulated surface defect is presented in Fig. 3(a). A photo depicting the fully assembled experimental sample is presented in Fig. 3(b), while Fig. 3(c) provides a schematic cross-sectional view of the experimental sample. DWTs in a 2 × 4 matrix were designed and fabricated to form the ultrasonic transducer array. The DWTs comprise a piezoelectric coating made of poly (vinylidene fluoride-trifluoroethylene) (P(VDF-TrFE)), silver electrode, and a protective layer, as illustrated in Fig. 3(c). The P(VDF-TrFE) layer was spray-coated onto the aluminum alloy block using an aerosol spray coating system, dried at 80 °C then annealed at 135 °C for 30 min. The final thickness of the P(VDF-TrFE) coating was approximately 25 μm. Then, corona poling was performed on the P(VDF-TrFE) coating. Next, the top electrode matrix was deposited with the help of a shadow mask and cured at 70 °C. Following that, thin wires were used to connect the top electrodes to a customized flexible printed circuit (FPC) with eight signal channels. The customized FPC was then connected to the ultrasonic testing system through a D-Subminiature (DB9) connector. Lastly, the DWT was encapsulated in the protective layer. The DWT was designed to be operated at an off-resonant frequency of 2 MHz, rather than its thickness-resonant frequency of 44 MHz. Operating at off-resonant frequencies is a well-established practice in ultrasonic SHM applications [13–18,2,3,6]. Although the absolute signal magnitude is smaller for off-resonance operation, this approach reduces signal ringing and harmonic distortion, enhancing the clarity of the signal. Furthermore, off-resonant operation allows greater adaptability for working frequency selection and for switching between different ultrasonic wave modes that can broaden the detection range for various structural defects.

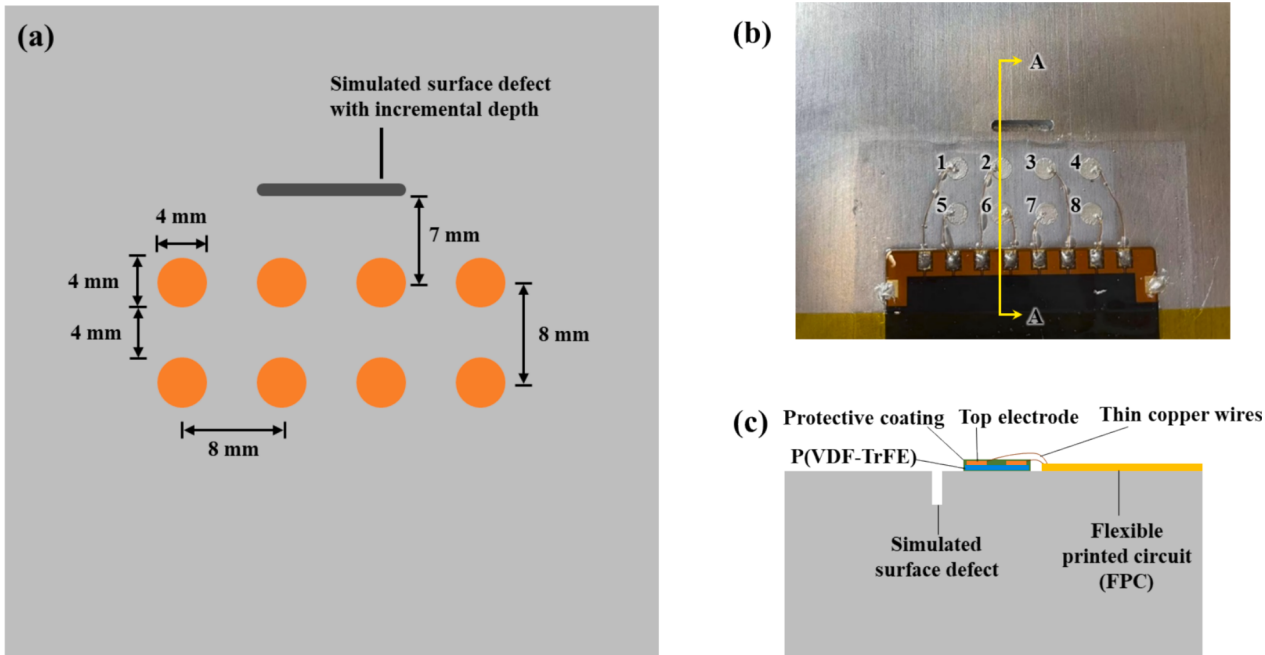


**Fig. 3.** (a) Schematic showing the top view of the aluminum alloy block, indicating the layout of the DWTs, and the dimensions and location of a surface defect; (b) photo of the fully assembled experimental setup with the 2 × 4 DWT matrix on the aluminum alloy block; (c) cross-sectional A-A view schematic of the DWT and the customized flexible printed circuit.

To evaluate and better understand the DWTs performance, both effective capacitance and effective piezoelectric coefficient ( $d_{33,eff}$ ) were measured using impedance analyzer (Agilent, 4294A) and laser scanning vibrometer (Polytec, PSV-400), respectively. Since the DWTs are fabricated directly onto the aluminum alloy block, removing them for capacitance measurement is impractical and would be irreversible. Therefore, capacitance measurements were conducted across each ultrasonic transducer's isolated top electrode, with the aluminum alloy block serving as the common ground. It should be noted that in this configuration, the aluminum alloy block mechanically constrains the DWT, resulting in a reduced measured capacitance compared to unconstrained conditions [19]. In addition, before measuring the effective capacitance, the open-and-short calibration was conducted to compensate for the parasitic effects that may be introduced by the measurement setup.

The  $d_{33,eff}$  was determined using the converse piezoelectric effect by scanning the top electrode area and its surrounding region [20]. As an example, the 3D displacement profile for UT7 is presented in Fig. 4. The effective capacitance and  $d_{33,eff}$  values measured for individual ultrasonic transducer are provided in Table 1. Based on the measurements, the average effective capacitance is 24.0 pF with a standard deviation of 2.3 pF, while the average measured  $d_{33,eff}$  is -17.8 with a standard deviation of 0.2 pm/V. The small standard deviations indicate uniformity in the DWTs and suggest effective scalability to form arrays with multiple ultrasonic transducer elements by the direct-writing method.

A slot with a fixed length and width of 12 mm and 2 mm, respectively, was machined with incremental depths using a milling machine. The depth increases by approximately 0.1 mm to 0.3 mm per iteration up to a maximum depth approximately 7.0 mm due to the length of the drill bit. These processes created a simulated crack for algorithm verification. The actual depth of the surface defect was measured using a depth gauge each time after the milling iteration. This was followed by an ultrasonic test with a research ultrasound platform (Verasonics, VANTAGE 64), carried out in full matrix capture (FMC) mode [21]. In FMC mode, one ultrasonic transducer is assigned as the ultrasonic wave transmitter, while all ultrasonic transducers serve as ultrasonic receivers in a round-robin manner, enabling the acquisition of the full matrix ultrasonic data. The experiment was conducted using a one-cycle sine wave excitation signal with a frequency of 2 MHz.

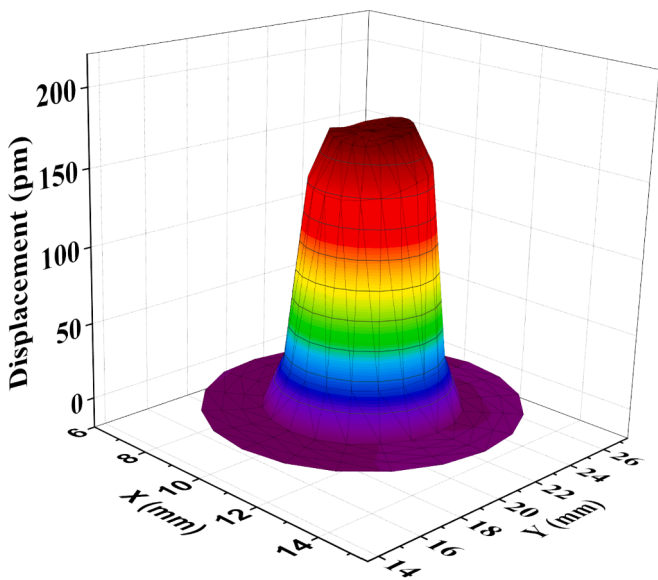


Fig. 4. Displacement 3D profile for UT7 measured using a laser scanning vibrometer.

**Table 1**

Effective capacitance and effective piezoelectric coefficient for the ultrasonic transducers.

Ultrasonic transducer	Effective capacitance (pF)	Effective piezoelectric coefficient, $d_{33,eff}$ (pm/V)
UT1	23.4	-17.5
UT2	24.3	-17.8
UT3	23.4	-17.8
UT4	25.6	-17.5
UT5	20.6	-17.8
UT6	20.2	-18.0
UT7	20.7	-18.1
UT8	22.6	-17.9

#### 4. Numerical simulation studies

To better visualize the propagation path of the TRBW within the structure and its interaction with the surface defect, 2D finite element (FE) models were developed using COMSOL, shown in Fig. 5. For simulation, the transmitter and receiver regions were modelled using mapped mesh, whereas the protective layer and aluminum alloy block were modelled using free quadrilateral mesh, with mesh size defined such that there were at least five elements per wavelength for accurate modelling of the ultrasonic wave propagation. In the simulation model, a fixed constraint was applied to the bottom surface of the aluminum block, and low-reflecting boundary conditions were applied to the top of the ultrasonic transducers, and perfectly matched layers were applied on the edges of the aluminum alloy block to avoid undesired wave reflections. The time domain analysis was conducted by using both the solid mechanics and electrostatic modules. The longitudinal bulk wave was induced by applying a one-cycle sine wave excitation with a frequency of 2 MHz as an electric potential to the excitation electrode boundary on the top of the transmitter. The interactions between TRBW and different surface defect sizes are investigated by conducting a parameter study. Simulations were carried out with combinations of surface defect dimensions, ranging from 0 to 10 mm in depth ( $d$ ) with increments of 1 mm.

To visualize the propagation of the TRBW, snapshots from simulations' results at different time intervals for a surface defect with width of 2 mm, and depth of 9 mm are given in Fig. 6(a). At  $t = 3 \mu\text{s}$ , the generated ultrasonic bulk wave travels towards the backwall of the structure and is reflected towards the tip of the defect. Upon reaching the tip at  $t = 11 \mu\text{s}$ , the ultrasonic bulk wave is diffracted. The diffracted ultrasonic wave then travels back towards the backwall before being reflected to the ultrasonic transducer and being detected as TRBW at  $t = 22 \mu\text{s}$ . The

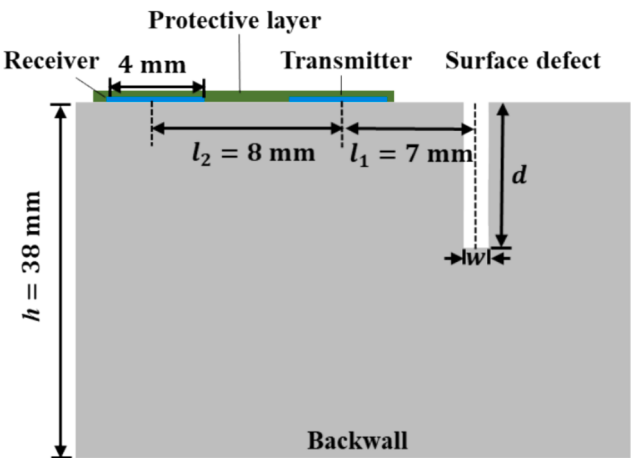
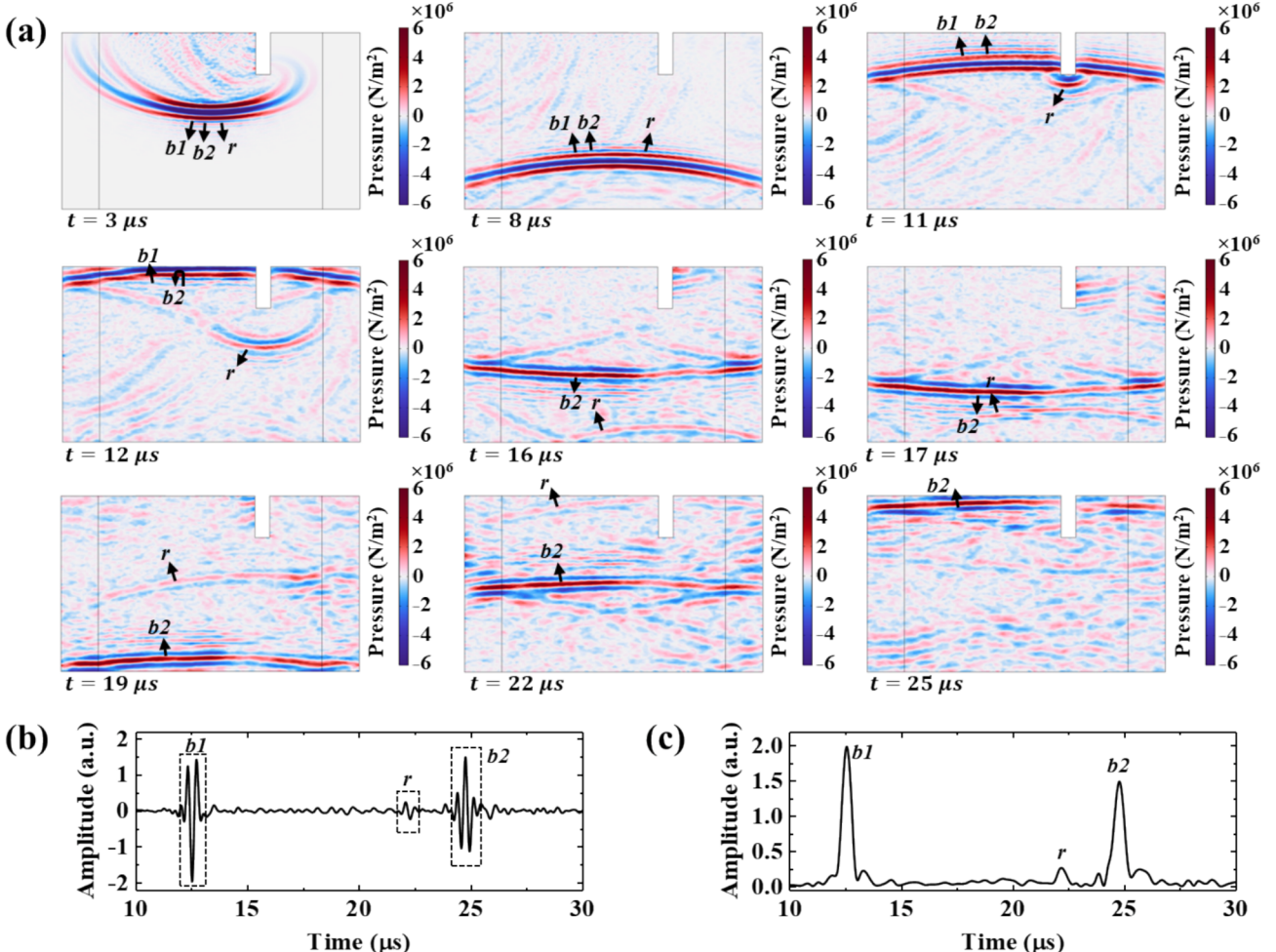


Fig. 5. Layout and dimensions for the 2D FE model, including an aluminum alloy block with a surface defect, longitudinal bulk wave transmitter and receiver at the same side of the defect on the same surface, and protective layer.



**Fig. 6.** (a) Snapshots from simulations' results at different time intervals for surface defect size of width 2 mm, and depth of 9 mm with the wavefronts of the first and second backwall reflections as well as the TRBW represented by  $b1$ ,  $b2$ , and  $r$ , respectively; (b) simulation time-domain signal showing ultrasonic signal detected by the receiver; (c) enveloped time-domain signal.

wavefront of TRBW is represented as  $r$ . Likewise, the wavefronts of the first and second backwall reflections are represented as  $b1$  and  $b2$ , respectively. Fig. 6(b) shows the simulation time-domain signal, with  $b1$ ,  $b2$ , and  $r$  detected by the receiver. The time-domain signal is then rectified and enveloped, as in Fig. 6(c), to clearly show the arrival time of the first and second backwall reflections as well as the TRBW as  $t_{b1} =$

$12.56 \mu\text{s}$ ,  $t_{b2} = 24.77 \mu\text{s}$ ,  $t_r = 22.16 \mu\text{s}$ , respectively.

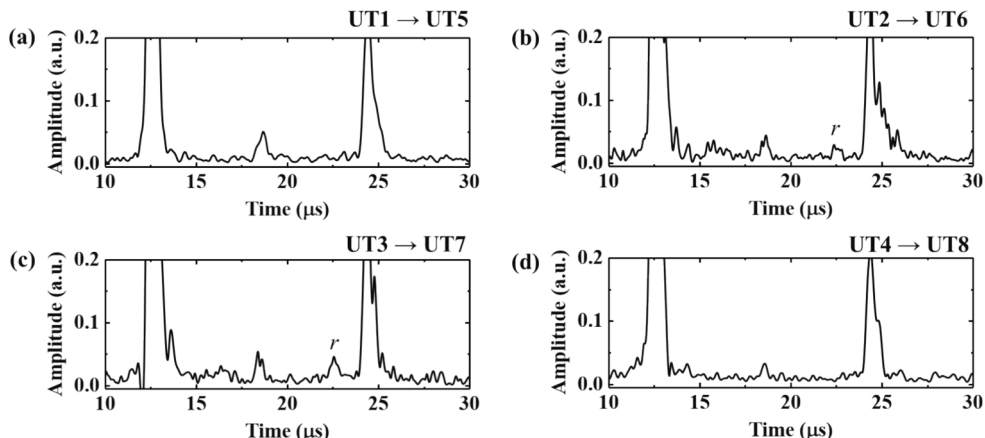


**Fig. 7.** Enveloped ultrasonic signals with surface defect depth of 6.90 mm located in front of UT2 and UT3, with TRBW marked as  $r$ , obtained by the following pair of UT in pitch-catch mode: (a) UT1 → UT5; (b) UT2 → UT6; (c) UT3 → UT7; (d) UT4 → UT8.

## 5. Results and discussion

### 5.1. Locating the surface defect

The ability of the TRBW algorithm to determine the location of the surface defect from the ultrasonic transducer array located at the same side is first demonstrated. In the experimental demonstration, the following pairs of ultrasonic transducers were tested in pitch-catch mode: UT1 → UT5, UT2 → UT6, UT3 → UT7, and UT4 → UT8 (ultrasonic transducers as labelled in Fig. 3(b)). Fig. 7 presents the enveloped ultrasonic signals when the surface defect has a depth of 6.90 mm located in front of UT2 and UT3. The enveloped ultrasonic signals for UT2 → UT6 and UT3 → UT7 detected a clear TRBW marked by *r* in Fig. 7(b) and (c), respectively. However, no clear TRBW signals were observed when using UT1 → UT5 and UT4 → UT8, shown in Fig. 7(a) and (d). This indicates that there is no surface defect in the near proximity of UT1 and UT5. The distance of the surface defect from UT2 can be estimated using Eq. (3) to be 6.91 mm, which is accurate.

### 5.2. Surface defect depth monitoring

Once the location of the surface defect is known, the depth of the surface defect can be monitored. For this demonstration, transmitter UT2 and receiver UT6 were used. The enveloped signals obtained from experiment can then be compared with the simulation results shown in Fig. 8. From Fig. 8 (a) and (b), the TRBW signals for both simulation and experiment, marked as *r*, would shift, indicating that the TRBW would arrive earlier as the surface defect depth increases. This is because as the surface defect depth increases, the travel path length of the ultrasonic bulk wave becomes shorter.

Simulation studies reveal that the minimum detectable depth of surface defects with this configuration is 3.0 mm, while experimental

results show a depth of 2.8 mm. From Fig. 8(c), the ultrasonic signals for 0 mm, 1 mm and 2 mm defect depths are similar, whereas the ultrasonic signal for 3 mm defect is much distinct, due to the presence of the TRBW signal labelled *r*. Similarly, experimental results demonstrate the ability to detect surface defects starting from 2.8 mm based on the ultrasonic signal. Fig. 8(d) shows the estimated surface defect depth from simulation and experimental results. The actual defect depth for the experimental results were measured by a vernier calliper. The surface defect depths estimated through both simulation and experimental results exhibit great agreement, demonstrating the capability of using TRBW to measure surface defect depth.

### 5.3. Surface defect mapping

Once the location of the surface defect is known, the DWT array matrix can be used to map and closely monitor the surface defect depth growth in pitch-catch mode: UT1 → UT5 (location 1), UT2 → UT6 (location 2), UT3 → UT7 (location 3), and UT4 → UT8 (location 4). The monitoring results are provided in Fig. 9, demonstrating that this approach allows the algorithm to map the incremental depth of the surface defect from 2.80 mm to 6.90 mm, showing great agreements with error less than 10 %. Although the spatial resolution may seem inadequate and discrete, it remains a computationally efficient means of hotspot monitoring. If necessary, additional ultrasonic transducers can be added to enhance the spatial resolution of the monitoring region. The direct-write fabrication method is particularly powerful to form array of transducers made from piezoelectric coating.

## 6. Future research directions

The relatively low signal amplitude of the TRBW signals from both the simulation and experimental results may be a concern in practical

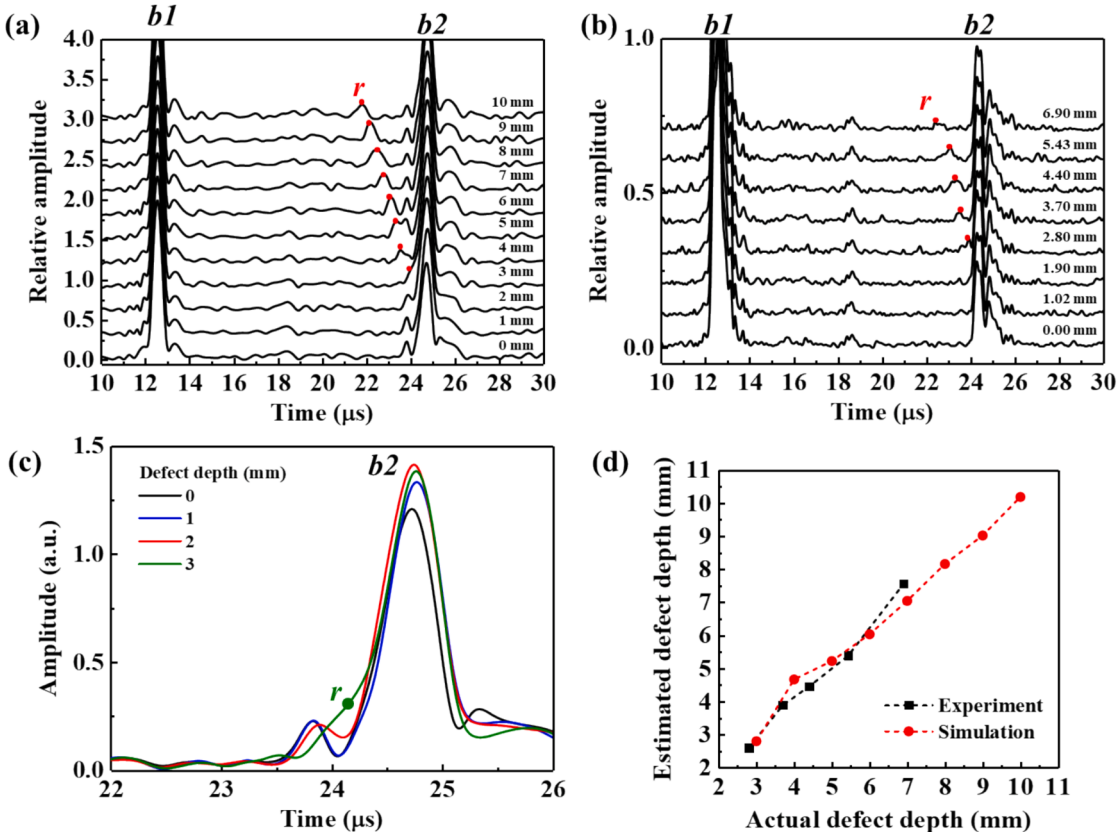


**Fig. 8.** (a) Simulation and (b) experimental ultrasonic signals for different surface defect depths using transmitter UT2 and receiver UT6; (c) zoom-in signal of the simulation results; (d) graph of estimated defect depth from simulation and experimental results against actual defect depth.

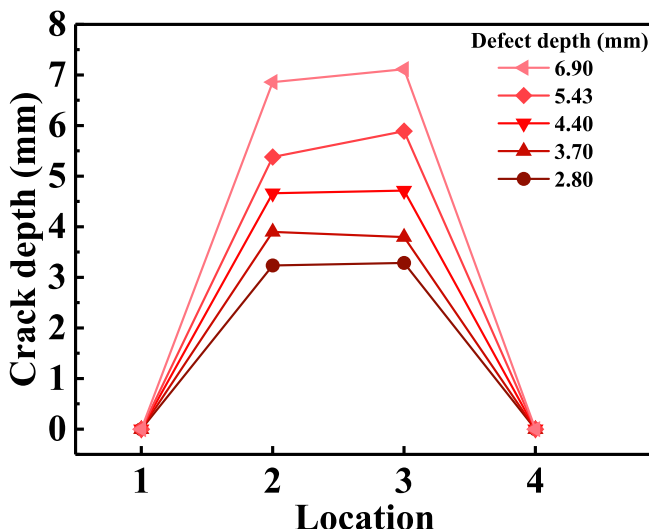


**Fig. 9.** Monitoring of the surface defect depth using the DWT array in pitch-catch mode: UT1 → UT5 (location 1), UT2 → UT6 (location 2), UT3 → UT7 (location 3), and UT4 → UT8 (location 4).

applications of the method proposed in this work. To address this, a pre-amplifier could be used to boost the amplitude of the received ultrasonic signal. In the current setup, the FPC connected to the ultrasonic testing system is shielded against electrical crosstalk and electromagnetic interference (EMI). However, the top electrodes of the DWT and the wires connecting to the FPC are unshielded. For practical applications, the thin wires and top electrodes could be incorporated to the FPC design offering more comprehensive shielding and thereby reducing signal noise. In addition, advanced post-processing techniques including training artificial intelligence models to distinguish the TRBW signals from the backwall reflections and noise could be a promising avenue for further exploration.

Another point of interest is the effect of variation in the surface defect geometries. In this work, the width of the machine surface defect is fixed at 2 mm for the methodology feasibility demonstration, and to ensure the numerical studies are consistent with the experimental tests. Future research work could involve investigating the effects of varying the distance between the ultrasonic transducers, defect width and angle (especially small widths and large angles) on the TRBW signals.

Improving the DWT design through numerical parametric studies is another area for future exploration. Parameters such as the shape or geometry of the top electrodes, the placement of DWT elements within the array, and variations in excitation voltage can be optimized. These enhancements are enabled by the flexibility of DWT fabrication that includes spray-coating of the piezoelectric layer and the deposition of custom-designed top electrode patterns directly onto the structure.

Positioning the DWT array on the same surface and at the same side of the surface defect makes this method suitable for surface defect monitoring in a wide range of engineering structures, particularly those with only single-sided access possible, such as welded joints. The DWT's conformability allows the transducer array to be applied to structures with complex geometries, including tubular or bent configurations. It will be of great interest for the future work cover scaled testing and developing ultrasonic SHM electronic systems that complement the TRBW method and DWT array design.

## 7. Conclusions

Through our theoretical analysis and experimental validation, a new method using twice reflected ultrasonic bulk wave (TRBW) excited and detected with in-situ fabricated conformable DWTs is developed to effectively monitor surface defect growth, in which the transducers are

conveniently located on the same surface and at one side of the defect. The algorithm is simplified using TRBW by establishing the quantitative relationship between tip diffraction signal arrival time and defect depth. With the tip diffraction signals in the TRBW method are highly distinguishable from other signals because of the extended arrival time, thus even very near surface defects are detectable. In our experimental verification, a DWT array of  $2 \times 4$  matrix was in-situ fabricated on an aluminum alloy block, and a slot with incremental depth was machined on the block as the simulated surface defect. The results showed that surface defects deeper than 2.80 mm were successfully detected and monitored, showing great agreements with error less than 10 %. With the transducers positioned on the same surface and at the same side, this TRBW method is generally applicable for surface defect monitoring of various engineering structures, including flat, tubular, bent, joint, or welded structures. When necessary, it is convenient to form DWT array to enhance the spatial resolution for mapping the defect profile.

## CRediT authorship contribution statement

**Voon-Kean Wong:** Writing – original draft, Visualization, Validation, Methodology, Investigation, Formal analysis. **Xiaotian Li:** Writing – original draft, Visualization, Validation, Software, Investigation, Formal analysis. **Yasmin Mohamed Yousry:** Investigation, Formal analysis. **Marilyne Philibert:** Software, Investigation, Formal analysis. **Chao Jiang:** Software, Formal analysis. **David Boon Kiang Lim:** Writing – review & editing, Visualization, Investigation. **Percis Teena Christopher Subhodayam:** Validation, Investigation. **Zheng Fan:** Writing – review & editing, Formal analysis. **Kui Yao:** Writing – review & editing, Formal analysis.

## Declaration of competing interest

The authors declare that they have no known competing financial interests or personal relationships that could have appeared to influence the work reported in this paper.

## Acknowledgements

This research is supported by A\*STAR under its RIE 2020 AME Industry Alignment Fund Prepositioning Programme (IAF-PP) (Grant No. A19F1a0104 and A20F5a0043) and a follow-up work IMNC230925aIMRCOL at IMRE.

## Data availability

Data will be made available on request.

## References

- [1] C.J. Hellier, *Handbook of Nondestructive Evaluation*, 3rd Edition, McGraw-Hill Education, New York, 2020.
- [2] V. Janapati, F. Kopsaftopoulos, F. Li, S.J. Lee, F.-K. Chang, Damage detection sensitivity characterization of acousto-ultrasound-based structural health monitoring techniques, *Struct. Health Monit.* 15 (2) (2016) 143–161, <https://doi.org/10.1177/1475921715627490>.
- [3] X. Li, V.-K. Wong, M. Yousry, D.B.K. Lim, P.T.C. Subhodayam, K. Yao, L. Feng, X. Qian, Z. Fan, Surface crack monitoring by Rayleigh waves with a piezoelectric-polymer-film ultrasonic transducer array, *Sensors.* 23 (5) (2023) 2665, <https://doi.org/10.3390/s23052665>.
- [4] G. Hévin, O. Abraham, H.A. Pedersen, M. Campillo, Characterization of surface cracks with Rayleigh waves: a numerical model, *NDT&E Int.* 31 (4) (1998) 289–297.
- [5] M.V. Felice, Z. Fan, Sizing of flaws using ultrasonic bulk wave testing: A review, *Ultrasonics* 88 (2018) 26–42, [https://doi.org/10.1016/S0963-8695\(98\)80013-3](https://doi.org/10.1016/S0963-8695(98)80013-3).
- [6] S. Mariani, Y. Liu, C. Peter, Improving sensitivity and coverage of structural health monitoring using bulk ultrasonic waves, *Struct. Health Monit.* 20 (5) (2020) 2641–2652, <https://doi.org/10.1177/1475921720965121>.
- [7] M.G. Silk, B.H. Lidington, The potential of scattered or diffracted ultrasound in the determination of crack depth, *Non-Destruct Test.* 8 (3) (1975) 146–151, [https://doi.org/10.1016/0029-1021\(75\)90024-9](https://doi.org/10.1016/0029-1021(75)90024-9).

- [8] F.W.T. Yeh, T. Lukomski, J. Haag, T. Clarke, T. Stepinski, T.R. Strohaecker, An alternative Ultrasonic Time-of-Flight Diffraction (TOFD) method, *NDT&E Int.* 100 (2018) 74–83, <https://doi.org/10.1016/j.ndteint.2018.08.008>.
- [9] S.J. Jin, X. Sun, Z.B. Luo, T.T. Ma, L. Lin, Quantitative detection of shallow subsurface cracks in pipeline with time-of-flight diffraction technique, *NDT&E Int.* 118 (2021) 102397, <https://doi.org/10.1016/j.ndteint.2020.102397>.
- [10] S. Baby, T. Balasubramanian, R.J. Pardikar, M. Palaniappan, R. Subbaratnam, Time-of-flight diffraction (TOFD) technique for accurate sizing of surface-breaking cracks, *Insight NDT & CM.* 45 (6) (2003) 426–430, <https://doi.org/10.1784/insi.45.6.426.52885>.
- [11] A. Zarei, S. Pilla, Laser ultrasonics for nondestructive testing of composite materials and structures: a review, *Ultrasonics* 136 (2024) 107163, <https://doi.org/10.1016/j.ultras.2023.107163>.
- [12] S.J. Jin, Z. Wang, Y. Yang, Z. Luo, Corrected mode-converted wave method for detecting defects in TOFD dead zone, *J. Nondestruct. Eval.* 42 (62) (2023), <https://doi.org/10.1007/s10921-023-00975-5>.
- [13] A. Shen, S. Chen, L. Zhang, K. Yao, C.Y. Tan, Direct-Write Piezoelectric Ultrasonic Transducers for Non-Destructive Testing of Metal Plates, *IEEE Sensors.* 17 (11) (2017) 3354–3361, <https://doi.org/10.1109/JSEN.2017.2694454>.
- [14] M. Philibert, S. Chen, V.-K. Wong, W.H. Liew, K. Yao, C. Soutis, M. Gresil, Direct-write piezoelectric coating transducers in combination with discrete ceramic transducer and laser pulse excitation for ultrasonic impact damage detection on composite plates, *Struct. Health Monit.* 21 (4) (2022) 1645–1660, <https://doi.org/10.1177/14759217211040719>.
- [15] V.-K. Wong, M. Liu, W.-P. Goh, S. Chen, Z.Z. Wong, F. Cui, K. Yao, Structural health monitoring of fastener hole using ring-design direct-write piezoelectric ultrasonic transducer, *Struct. Health Monit.* 21 (6) (2022) 2657–2669, <https://doi.org/10.1177/14759217211073950>.
- [16] S. Guo, S. Chen, L. Zhang, Y.F. Chen, K. Yao, Plastic strain determination with nonlinear ultrasonic waves using in situ integrated piezoelectric ultrasonic transducers, *IEEE t. Ultrason. Ferr.* 65 (1) (2017) 95–101, <https://doi.org/10.1109/TUFFC.2017.2768238>.
- [17] S. Guo, S. Chen, L. Zhang, Y.F. Chen, M.S. Mirshekarloo, K. Yao, Design and fabrication of direct-write piezoelectric ultrasonic transducers for determining yielding of aluminum alloy, *NDT&E Int.* 98 (2018) 186–194, <https://doi.org/10.1016/j.ndteint.2018.05.009>.
- [18] T.R. Hay, J.L. Rose, Flexible PVDF comb transducers for excitation of axisymmetric guided waves in pipe, *Sens. Actuators, A.* 100 (1) (2002) 18–23, [https://doi.org/10.1016/S0924-4247\(02\)00044-4](https://doi.org/10.1016/S0924-4247(02)00044-4).
- [19] N. Elvin, A. Elvin, B.Z. Senderos, Capacitance changes in thin piezoelectric transducers embedded in isotropic host materials, *J. Intell. Mater. Syst. Struct.* 29 (5) (2018) 816–829, <https://doi.org/10.1177/1045389X17721045>.
- [20] K. Yao, and F.E.H. Tay, Measurement of longitudinal piezoelectric coefficient of thin films by a laser-scanning vibrometer, *IEEE T. Ultrason. Ferr.* 50(2) (2003) 113–226, <https://doi.org/10.1109/TUFFC.2003.1182115>.
- [21] X. Sun, A.J. Croxford, B.W. Drinkwater, Continuous monitoring with a permanently installed high-resolution ultrasonic phased array, *Struct. Health Monit.* 22 (5) (2023) 3451–3464, <https://doi.org/10.1177/14759217231152413>.